Research Square

Preprints are preliminary reports that have not undergone peer review.
They should not be considered conclusive, used to inform clinical practice,
or referenced by the media as validated information.

Airborne Exposure of Human Primary Alveolar Cells to Benzo[a]pyrene Induces Acute Cellular Stress and Remodeling

Sem Koornneef
Sophia Children's Hospital, Erasmus Medical Center
Cinta Iriondo Martinez
Sophia Children's Hospital, Erasmus Medical Center
Jingshu Zhang
Erasmus Medical Center
Marjon Buscop-van Kempen
Sophia Children's Hospital, Erasmus Medical Center
Anne Boerema-de Munck
Sophia Children's Hospital, Erasmus Medical Center
H. Bing Thio
Erasmus Medical Center
J. Marco Schnater
Sophia Children's Hospital, Erasmus Medical Center
Robbert J. Rottier
r.rottier@erasmusmc.nl

Sophia Children's Hospital, Erasmus Medical Center

Research Article

Keywords: human primary alveolar cells, Air-liquid interface culture, apical exposure, nebulization, Transcriptomics, Benzo[a]pyrene

Posted Date: November 23rd, 2026

DOI: https://doi.org/10.21203/rs.3.rs-11798823/v1

License: This work is licensed under a Creative Commons Attribution 4.0 International License.
Read Full License

Additional Declarations: No competing interests reported.

AIRBORNE EXPOSURE OF HUMAN PRIMARY ALVEOLAR CELLS TO BENZO[A]PYRENE INDUCES ACUTE CELLULAR STRESS AND REMODELING

Sem Koornneef[1,2,4], Cinta Iriondo Martinez[1,2], J. Zhang[3], Marjon Buscop-van Kempen[1,2], Anne Boerema-de Munck[1,2], H. Bing Thio[4], J. Marco Schnater[1], Robbert J. Rottier[1,2]*

[1]Department of Pediatric Surgery, Sophia Children's Hospital, Erasmus Medical Center, Rotterdam, The Netherlands

[2]Department of Developmental & Cell Biology, Erasmus Medical Center, Rotterdam, The Netherlands

[3]Department of Viroscience, Erasmus Medical Center, Rotterdam, The Netherlands

[4]Department of Dermatology, Erasmus Medical Center, Rotterdam, The Netherlands

*Corresponding author

Robbert J. Rottier,

ORCID ID: 0000-0002-9291-4971

Erasmus MC-Sophia Children's Hospital, Dept Pediatric Surgery

Wytemaweg 80, 3015 CN Rotterdam, the Netherlands

e-mail: r.rottier@erasmusmc.nl

Keywords: human primary alveolar cells, Air-liquid interface culture, apical exposure, nebulization, Transcriptomics, Benzo[a]pyrene

Abstract

The majority of world's population is exposed to air pollution levels that exceed WHO guidelines. Air pollution poses a significant threat to human respiratory health. Fine and ultrafine particles can penetrate deep into the respiratory tract and reach the alveoli, the primary site of gas exchange in the lung. As a result, the alveolar epithelium is particularly vulnerable to inhaled toxic pollutants. In this study, optimized Air-liquid interface (ALI) cultures of human primary alveolar cells were apically exposed to either a single, high-dose or to repeated low-doses of benzo[a]pyrene (BaP), a major constituent of air pollution, to mimic acute and chronic exposure, respectively. Transcriptomic analyses revealed enriched pathways of DNA repair and oxidative phosphorylation after acute or chronic exposure. Remarkably, only chronic exposure induced changes in inflammatory signaling and epithelial remodeling signatures, including enhanced DNA repair and altered mitochondrial activity. These findings were supported by immunofluorescence staining of the proliferative marker Ki67 and DNA damage marker γ-H2AX.

Collectively, our data demonstrate that human primary alveolar cells are physiologically relevant to model airborne pollutant exposure and our studies highlight the importance of chronic exposure models for studying the impact of air pollutants. Interestingly, chronic exposure of primary alveolar cells elicited a qualitatively distinct response from acute exposure, and suggests that chronic exposure brings alveolar cells in a primed immunological state. This could have clinical implications as people living in polluted areas may be more vulnerable and at higher risk to additional triggers.

Introduction

Air pollution affects almost every person around the globe. The State of Global Air estimates that around 36% of the worldwide population is exposed to an exceeding amount of 35 μg/m^3 of air pollutants, especially fine particulate matter of 2.5 μm and smaller (PM2.5)((HEI) 2025). This is already exceedingly more than the advised maximal annual level of 5 μg/m^3 present in almost all inhabited places on earth((WHO) 2021). Air pollutants are the second largest risk factor for death worldwide after high blood pressure((HEI) 2025). It consists of a wide variety of organic and inorganic compounds of which the composition differs depending on the time of year and geographical location(Chen et al. 2023; Koornneef et al. 2025; van Donkelaar et al. 2019). Due to their small size, many airborne pollutants can penetrate deep into the respiratory tract and reach the vulnerable alveolar region of the lung.

The lung is an essential organ for life as its main purpose is to serve as a gas exchange organ. Inhaled oxygen rich air is transported via the trachea, bronchi and bronchioles to the alveoli. The O_2 and CO_2 exchange between the inhaled air and the gas-carrying erythrocytes in the blood takes place through the epithelium-covered luminal space, the basement membrane and the endothelial covered capillaries aligning next to the alveoli(Whitsett et al. 2019). The alveolar epithelium consists of alveolar type 1 (AT1) and type 2 (AT2) cells in almost equal numbers, but the flat AT1 cells cover 95% of the surface(M. Ochs 2019). The cuboidal AT2 cells produce surfactant to reduce the surface tension in the alveoli and serve as the main progenitors for the AT1 cells(Burgess et al. 2024).

As the alveolar region possesses an extensive surface area of around 100 m^2, it is particularly vulnerable to interactions with inhaled pollutants(M. Ochs 2019). The toxic compounds present in air pollution can damage the alveoli and subsequently be taken up into the bloodstream(Olesiejuk and Chalubinski 2023). Despite their central role in pulmonary toxicology, studying human alveolar epithelial responses remains challenging as collecting and growing primary cells remains difficult. Air pollution studies are often conducted on animals or immortalized alveolar cells(Sengupta et al. 2023; Yang et al. 2025). While animal models provide valuable insights into inhalation toxicology, species-specific differences in lung anatomy, particle deposition, and immune responses can limit the translation of findings to humans(Lin et al. 2022). In addition, immortalized cell models are highly reproducible and relatively easy to maintain, they often exhibit altered cellular signaling, transcriptional regulation, and metabolic activity, limiting their physiological relevance for toxicology studies(Suali et al. 2026). Therefore, more physiological relevant human alveolar models are required to study the effect of inhaled pollutants.

In recent years, primary cells and induced pluripotent stem cell (iPSCs)-derived alveolar-like cells have been successfully grown to provide more insights into their lineages(Burgess et al. 2024; Li et al. 2024; Ohnishi et al. 2024). Although alveolar cells are difficult to culture in 2D, AT2 cells can be maintained as organoids and have the ability to differentiate into AT1-like cells(Burgess et al. 2024; Li et al. 2024; Ohnishi et al. 2024). So, these cells therefore provide a valuable platform for studying human lung biology, diseases and environmental exposures.

AT2 cells cultured as organoids can be exposed to pathogens or toxicants in 3D culture. However, their application in air pollution studies is limited because the cells are embedded within a 3D matrix and the apical surface is predominantly oriented towards the organoid lumen, restricting direct exposure to airborne pollutants. To better recreate the *in vivo* alveolar structure, Air-liquid-interface (ALI) models are used in which the alveolar cells are grown on a porous membrane insert allowing the cells to be exposed to air apically and nutrients are taken up at the basolateral side(Grytting et al. 2024). The ALI cultures can apically exposed to air pollutants through nebulization(Grytting et al. 2024). Nevertheless, current alveolar ALI models still lack robust long-term maintenance of both AT2 and AT1 cells, highlighting the need for further optimization of culture conditions. A robust alveolar ALI model would not only improve the study of alveolar biology but also enable physiologically relevant investigations of airborne toxicants. This is particularly relevant for air pollution research, where inhaled compounds interact with the alveolar epithelium via the apical surface(Koornneef et al. 2025).

Benzo[a]pyrene (BaP) is a polycyclic aromatic hydrocarbon generated during combustion processes and a major constituent of PM2.5(Bukowska et al. 2022). Following exposure, BaP activates the aryl hydrocarbon receptor (AhR) pathway leading to oxidative stress, DNA damage and cell signaling alterations(Bukowska et al. 2022). Frequently, *in vitro* studies have focused on acute high dose exposures, whereas real life exposures are more long-term low dose exposure periods(Huang et al. 2023; Ryu et al. 2023; Wang et al. 2015). Consequently, it remains unclear whether repeated low dose BaP exposure induces the same transcriptional responses as acute high-dose exposure or whether adaptive mechanisms emerge during prolonged exposure.

We hypothesized that prolonged exposure to low BaP doses would induce distinct transcriptional responses compared with acute exposure, reflecting cellular adaptation processes within the epithelium. To test this hypothesis, we established and characterized a robust human primary alveolar ALI model to study the effects of long-term air pollution via BaP exposure. Primary alveolar cells were isolated from human lung tissue and expanded as organoids before transfer to ALI. Culture conditions were optimized to support long-term growth and reproducible toxicological assessment. Long-term pollution was stimulated by nebulization of air pollution compound BaP and analyzed for transcriptional responses for the acute and repeated BaP exposures. Analysis of pathways was further validated using immunofluorescence.

Results

Human alveolar organoid growth in culture: a comparison

Human alveolar organoids were generated from distal human primary lung tissue. Unsorted cells were initially grown in alveolar organoid medium (AOM)(Ebisudani et al. 2021; Nikolic et al. 2017) which resulted in the formation of dense, spherical structures (Figure 1A) and a low yield (<10%) when the AT2 cells were FACS sorted using the HT2-280 cell membrane marker. Although FACS sorting substantially reduced the number of airway organoids, airway organoids gradually reappeared and frequently outgrew the alveolar organoids during subsequent culture in AOM.

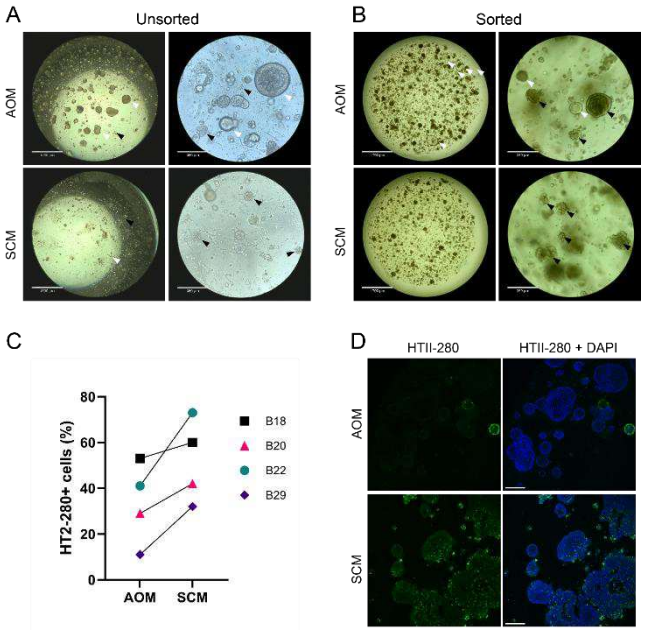

Figure 1: Comparison of AT2 organoids grown in AOM and SCM.

A: Representative bright field images of unsorted organoids (Donor B29, P0). White arrowheads indicate airway organoids; black arrowheads indicate alveolar organoids. Scale bar (left) = 1790 µm. Scale bar (right) = 360 µm.

B: Representative bright field images of FACS-sorted AT2 cells. White arrowheads indicate airway organoids; black arrowheads indicate alveolar organoids. Scale bar (left) = 1790 µm. Scale bar (right) = 360 µm. (Donor B18, P7)

C: FACS analysis of alveolar organoids cultured in AOM or SCM. The percentage of HT2-280+ cells after FACS sorting are shown for the alveolar culture grown in AOM or SCM. (Donors used: B18-square, B20-circle, B22-triangle, B29-diamond)

D: Representative images of an IF staining of AT2 organoids of FACS-sorted AT2 cells with antibodies against the AT2 marker HTII-280 (green), after 3 weeks of culture. Scale bar = 200 µm. (Donor B22)

To assess whether culture conditions contributed to this observed preferential growth of airway organoids, organoids were cultured in alveolar StemCell Medium (SCM). Compared to AOM, organoids cultured in SCM displayed a slower growth rate when seeded at similar densities (Figure 1A). However, following FACS sorting for HT2-280+ cells, the resulting organoids appeared more homogenous in morphology (Figure 1B).

To further compare both culture media, different donors grown in AOM and SCM were analyzed for HT2-280+ cells. FACS analysis of multiple donors demonstrated a trend toward a higher proportion of HT2-280+ cells in organoids cultured in SCM compared to AOM (Figure 1C). Consistent with the brightfield observations, organoids cultured in AOM more frequently displayed more airway-like organoids (Figure 1B, white arrows). Organoid expansion and subsequent sorting for HT2-280 efficiency remained donor dependent, with younger donors generally yielding higher numbers of HT2-280+ cells (Figure 1C).

Immunofluorescence (IF) staining of these cultures confirmed a higher proportion of HT2-280+ organoids in the SCM grown cultures, while the signal in AOM organoids was often restricted to individual spheres within mixed organoid populations (Figure 1D). The larger and denser airway organoids observed in AOM showed increased TP63+ signal, while organoids with TP63+ signal could not be detected in the SCM (Figure S1). Organoids grown in both media were positive for KRT5.

Overall, SCM produced a more homogenous alveolar organoid population enriched for HT2-280+ cells, whereas AOM promoted formation and expansion of TP63+ airway-like organoids despite repeated FACS enrichment.

Alveolar-like cultures on inserts

To enable apical exposure to airborne compounds, the AT2 cells derived from the alveolar organoids were transferred to ALI cultures. To facilitate future studies of epithelial-endothelial interactions at the alveolar-capillary barrier, which more closely resembles physiological alveolar microenvironment, we setup a workflow to co-culture microvascular endothelial cells and alveolar cells (Figure S2A), as performed previously with airway co-cultures(Iriondo et al. 2024).

Initially, cultures were seeded at a density of 2×10^5 cells per 24-well insert as used previously by Daum et al(Daum et al. 2012). For the growth of both cell types, their respective media, SAGM (AT2) and EGM-2MV (EC) were mixed at ratios of 2:1 and 1:1 and evaluated. The 2:1 medium better supported alveolar cells as determined by the expression of *RAGE* and *HOPX1* (AT1) and *SFTPC* and *LPCAT1* (AT2) when compared to the 1:1 medium (Figure S2B).

Retention of the endothelial cells was observed in both culture conditions after 2 weeks of culture, as indicated by CD31 and ERG1 expression (Figure S2C). Although CD31 expression appeared somewhat higher in the 1:1 condition, the substantially higher expression of alveolar markers in the 2:1 medium indicated better support of the alveolar epithelial phenotype (Figure S2B). Therefore, 2:1 medium was selected for subsequent experiments.

Expression of AT1 and AT2 specific genes changed over time (Figure S2D). The single alveolar cultures expressed more *SFTPC* after 3 weeks at ALI whereas the *LPCAT* expression decreased. The expression of the AT1-specific genes, *HOPX* and *RAGE,* did not vary over time. The expression of the alveolar-specific genes was consistently lower in co-culture conditions. Therefore, we further conducted this study using mono grown cultures.

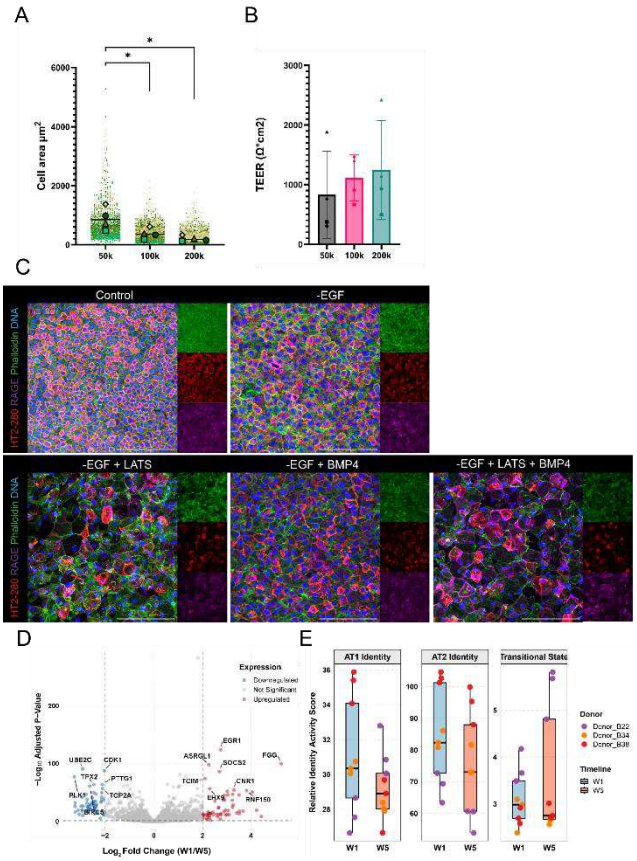

Figure 2: Optimalization of Alveolar-like ALI cultures on insert. A: Projected cell surface area and **B:** TEER of AT2-like cultures on insert plated at 0.5×10^5, 1×10^5 and 2×10^5 cells/insert (50k, 100k, 200k). The cells were grown for 2 weeks on ALI. N=4 (Donor B31-diamond, B32-circle, B33-square, B34-triangle) **C:** Representative images of IF staining of cultures grown with different media to test the differentiation of AT2 to AT1-like cells. Cells were seeded in a density of 0.5×10^5 cells per 24 well insert. Base medium and control consisted of SAGM 2% FCS:EGM-2MV in a 2:1 ratio. EGF was deleted in favor of BMP4 (100 ng/ml) or LATS-IN-1 inhibitor TRULI (10 µM) (Donor B38). Antibodies were used against the AT1 marker RAGE (purple) and the AT2 marker HT2-280 (red), and cell structures were directly visualized with phalloidin (filamentous actin; green) and DAPI (DNA, blue). **D:** DEG volcano plot analysis of 1 week ALI cultures (control start) compared to 5 weeks ALI (control end). Log2fold cut offs are set to 2 resulting in 61 upregulated genes and 60 downregulated genes. (Donor B22, B34, B38) **E:** Deconvolution DeCoupleR analysis of AT1, AT2 or transitional markers present in the samples over the four week time period. W1 and W5 are respectively week one and week five of ALI cultures. (Donor B22, B34, B38)

Next, the alveolar ALI cultures were initiated at three different cell densities, 0.5×10^5, 1×10^5 and 2×10^5 cells per 24 well insert, as suggested recently (Figure 2A)(Burgess et al. 2024). Significant differences in mean cell area were observed between seeding densities. Cultures seeded at 0.5×10^5 cells per insert exhibited significantly larger cell area coverage, which better mimicked the area size of *in vivo* surface area of the AT1 cells. The Trans Epithelial Electrical Resistance (TEER) measurements remained comparable between conditions (Figure 2B).

Overall, cultures seeded at 0.5×10^5 cells per insert exhibited the largest cell areas while maintaining TEER values comparable to higher seeding densities, and therefore used for all subsequent experiments.

Cultures grown for 2 weeks at ALI presented a mixed population of both AT2 and AT1-like cells according to immunofluorescence staining for HT2-280 and RAGE. As most of the alveolar lung surface area is covered with AT1 cells, we aimed to improve the differentiation of AT2 cells towards AT1-like cells. The control condition presented a mixed population of AT1, AT2 and transitionary cells (Figure 2C). Two potential small molecules were tested: a LATS kinase inhibitor - TRULI, and the morphogen BMP4. Both TRULI and BMP4 were shown in organoid cultures to increase the expression of AT1-specific markers(Li et al. 2024; Ohnishi et al. 2024). Addition of LATS inhibitor increased the size of the cells, but decreased the viability of most of the tested donors. Similarly, the TEER decreased to zero when the LATS inhibitor was added to the cultures (Figure S2E). Supplementation of BMP4 reduced the proportion of HT2-280+ cells, although no obvious increase in cell size was observed. The combination of the LATS inhibitor and BMP4 increased the size of the cells, but decreased the viability of most of the donors tested as determined by the detachment of the cells from the membranous support. Therefore, subsequent experiments were performed using the control condition due to its superior morphological stability and reproducibility across donors.

Next, we further explored the differentiation of the cultures and isolated RNA from alveolar ALI cultures at 1 week and at 5 weeks at ALI. RNAseq of these samples and subsequent principal component analysis (PCA), revealed a clear donor difference, in each donor clustered separately from each other and the one week ALI separated from the 5 weeks at ALI (Figure S2F). Comparison of significantly expressed genes between the 1 week and 5-week at ALI conditions revealed 121 Differentially Expressed Genes (DEGs). Most DEGs that were downregulated in the 5-week ALI were regulators of cell cycle transitions, like *CDK1*, and *CCNB*-family genes, and *KI67*. Moreover, *KRT4* and *KRT13* present in stratified/squamous lineages were downregulated as well. Other genes that are more related to cytokine signaling and environmental stress are upregulated, such as *EGR1*, *CXCL2*, *CXCL13* and *MMP1*. This suggests that the maturation of the epithelium with the differentiation of AT2 cells to AT1 cells, is accompanied by reduced proliferation and increased stress/remodeling signaling. This trend is also reflected in the Gene Set Enrichment Analysis (GSEA) analysis, in which epithelial to mesenchymal transitions (EMT) and inflammatory response signaling pathways are upregulated in the later control stages and mitotic spindle pathways and G2m checkpoint signaling is downregulated (Figure S2G). To visualize the systemic upstream regulatory shifts a DeCoupleR analysis was performed on the complete vector of gene level statistics (DESeq2 Wald t-statistics). Consistent with our observed DEGs, a DeCoupleR analysis of upstream regulators inferred a downregulation of *E2F2* and *E2F5* transcription factors for cell cycle progression and mitosis, complemented by a predicted increase of EGFR/MAPK signaling (Figure S2H).

To investigate whether these transcriptional changes were accompanied by shifts in alveolar identity, a deconvolution proxy was performed on a subset of marker genes related to the AT1, AT2 or transitional phenotypes (Figure 2E)(Supplementary table 1). At week 1 of ALI culture, cells demonstrated high baseline activity for AT1 and AT2 lineage markers. Over the 5-week timeline, both identity scores declined, accompanied by a progressive enrichment of the transitional state signature. Comparing within the different cell groups, we see donor dependent differences. While donor B22 increases in AT1 identity throughout the experiment, the other two donors decrease. In the AT2 identity plot, we see a decrease for all donors. In the transitional state, the B22 donor massively increases from start to end while the other two donors generally stay the same overtime.

Across donors, prolonged ALI culture was associated with a reduction of AT2 and AT1-like signatures, although the magnitude of these changes differed per donor.

Long-term exposure to Benzo[a]pyrene

We cultured our alveolar cells at ALI for 1 week before starting the BaP exposure. For the long-term exposure, ALI cultures were exposed twice weekly for 4 weeks (Figure 3A). During this period, the cells received eight low-dose BaP exposures (0.73 µM), accumulating to a total of 5.8 µM. To ensure identical culture duration and harvesting timepoints between exposure groups, short-term cultures received a single 5.8 µM BaP exposure concurrently with the final low-dose exposure of the long-term group.

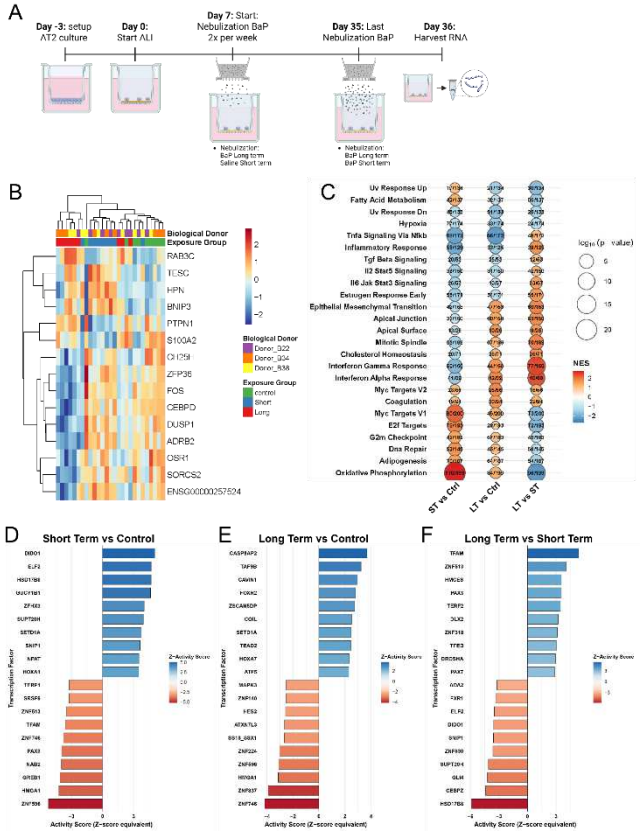

Figure 3: Bulk RNA-seq data for the comparisons of different exposure groups. A: Schematic overview of the conducted experiment. Used donors are B22, B34, B38, n=3. **B:** Expression profiles of the top variable expressed genes found in the 3 exposure groups. Values are expressed as z-scores, indicating a number above or below the population mean. **C:** GSEA for the different comparisons, the color code indicated in the heatmap is the normalized enrichment score, the size of the bubble is the log(p-value) and the number in the bubble is the actual active genes driving the enrichment in that specific condition. **D-F:** DecoupleR upstream profiles of the master transcription regulators of the short-term **(D:)** or long-term **(E:)** BaP exposure compared to the control situation and the long-term compared to the short-term exposure of BaP **(F:)**.

Cultures were harvested 24 hours later. RNA bulk sequencing was performed and PCA revealed separation of the 3 different cultured donors (Figure S3A). Within each donor, we found different clusters of controls, short-term and long-term exposures. However, removing the donor variability in the PCA plot did not result in clear

separation of the short exposure, long exposure and control groups (Figure S3B). Hierarchical clustering of the most variable genes resulted in separation of the three experimental conditions (Figure 3B). Unlike the PCA analysis, samples clustered primarily according to BaP exposure rather than donor identity, suggesting that the exposure-related transcriptional changes contributed substantially to the observed variation.

The heatmap of the top fifteen variable genes reveals a portion of genes (*RAB3C, TESC, HPN, BNIP3, PTPN1*) with relatively higher expression in both the short and long-term exposure group while down in the control group. In contrast, *FOS, DUSP1, CEBPD, ZFP36, ADRB2, OSR1* and *SORCS2* displayed relatively lower expression in the long-term exposure condition than in the short-term and control groups. While this heatmap provides an insight in the relative z-score compared over the different samples, it does not include insights in the differentially expressed up and downregulation of the genes itself.

Overall, relatively few genes passed both the False Discovery Rate (FDR) threshold and a log2 Fold Change (FC) cutoff of ±0.5, indicating that BaP exposure induced modest changes at the level of individual gene expression (Figure S3C-D). In the short-term compared to control conditions, *S100A2 PTPN1, HPN, BNIP3* and *TESC* were found to be above the FDR threshold but did not have a FC higher or lower than 0.5. Comparison of the long-term exposure and control condition, revealed that *RAB3C* was upregulated, while *FOS, SORCS2 and OSR1* are downregulated (Figure S3D, table 1). Comparing the long-term against the short-term *FOS*, and *WIF1* showed a downregulation of, and an upregulation of *IFI27* (Figure S3E). Many of the genes altered in both exposure conditions are associated with cellular stress adaptation, mitochondrial regulation and epithelial remodeling.

Gene set enrichment analysis of the short-term compared to the control displays significant upregulation in the DNA repair and oxidative phosphorylation pathways (Figure 3B, table 1). Downregulation of inflammatory response pathways like TNFa, interferon gamma and alpha responses. Moreover EMT appeared to be downregulated as well, similar to the apical junctions pathway. While in the comparison between the long-term exposure and control condition, interferon alpha/gamma responses, DNA repair and oxidative phosphorylation pathways were upregulated. In addition, enrichment of EMT-associated genes were observed, suggesting epithelial remodeling. Genes involved in apical junction organization and cell-cell interactions were also enriched, indicating alterations in epithelial barrier-related processes. Long-term exposure compared to the short-term exposure displays stronger enrichment of interferon alpha/gamma and TNFa responses, while oxidative phosphorylation and DNA repair pathways were downregulated. Similarly, EMT and apical junction pathways were enriched, suggesting increased epithelial remodeling and altering of the barrier regulation following repeated exposure. Overall, prolonged exposure to BaP was associated with increased interferon signaling, EMT related pathways, and apical junction-associated genes when compared to the acute short-term exposure.

The three different comparisons, short or long exposure compared to control, and long-term exposure compared to control, were analyzed using the DeCoupleR upstream analysis to find sets of genes with common transcription factor binding sites (TFs) in their genomic region (Figure 3D-F)(Table 1). In the short-term to control comparison, the most upregulated scores are DIDO1, ELF2, HSD17B8 respectively involved in metabolism and apoptosis, cell proliferation and chromatin remodeling, and hormone and mitochondrial metabolism(Garcia-Domingo et al. 2003; Guan et al. 2017; Lu et al. 2024). While ZNF596 and HMGA1, involved in gene transcription and expression, are downregulated. Long-term compared to control condition showed upregulation of CASP8AP2 and TAF9B (Figure 3E). This suggests increased regulation of apoptotic and transcriptional response pathways following prolonged exposure(Catalanotto et al. 2024; Pan et al. 2019). We find downregulation of similar TFs

as in the short-term comparison together with other ZNF family members. The comparison between long-term and short-term exposures revealed an upregulation of TFAM and HMCES(Rong et al. 2021; Srivastava et al. 2020). Consistent with the GSEA results, TFAM and HMCES activity increased in the long-term versus short-term comparison, suggesting enhanced regulation of mitochondrial maintenance and DNA repair processes during prolonged exposure. Downregulation of HSD17B8 and CEBPZ may contribute to attenuation of stress-response signaling and transcriptional regulation.

Collectively, these analyses indicate that BaP exposure induces relatively modest gene-level changes but consistent pathway level shifts. While both exposure regimens activated pathways associated with oxidative stress and DNA repair, the long-term exposure condition displayed features of enhanced inflammatory signaling, epithelial remodeling and chronic cellular adaptation not observed in the short-term exposure condition.

Short-term Benzo[a]pyrene exposure increases proliferation and DNA damage markers

Based on the RNA-seq data, changes in proliferation and DNA damage following BaP exposure were further investigated. ALI cultures were exposed according to the same experimental design used for the RNA sequencing (Figure 3A), and subsequently stained for the proliferation marker Ki67 and the DNA double strand break marker γ-H2AX. In addition, RAGE staining was included to assess the presence of AT1-like cells.

Comparable RAGE staining was observed across all exposure conditions, indicating that the alveolar phenotype was maintained following short and long-term exposure (Figure 4A). In contrast, differences were observed in γ-H2AX staining. γ-H2AX foci were detected in all conditions, but were generally more abundant in the short-term exposure group, than in either the saline control of long-term exposure group (Figure 4B). Long-term exposed cultures displayed γ-H2AX levels that were largely comparable to control cultures.

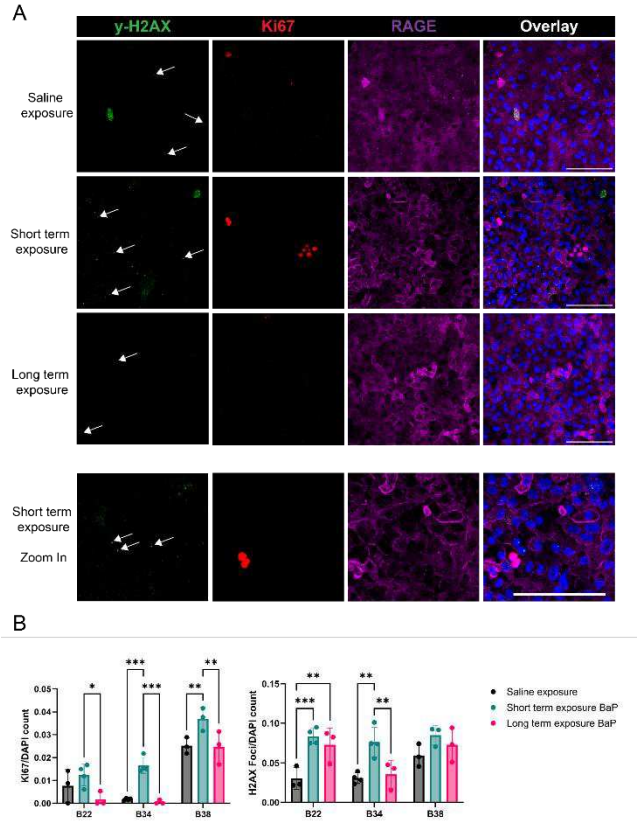

Figure 4: BaP exposure increases proliferation marker Ki67 and γ-H2AX marker for double strand breaks for three different donors. A: Representative images of IF staining of control, short-term and long-term exposures cultures with antibodies against γ-H2AX (green), Ki67 (red) and RAGE (purple). γ-H2AX marks the double strand breaks, Ki67 stains the proliferating cells, RAGE stains the AT1 cells. The white arrows mark the double strand breaks. Donor B34, scalebar is 100 μm. **B:** Quantification of the expression of Ki67+ cells and γ-H2AX foci normalized to the number of DAPI positive cells. 2-way ANOVA with Tukeys multiple comparisons test was used for significance testing. Adjusted p-values are plotted *p*: * ≤ 0.05, **≤ 0.01, ***≤ 0.01 n=3 (Donor B22, B34, B38)

Differences were also observed for Ki67 staining (Figure 4A). Short-term BaP exposure increased the number of Ki67-positive cells compared with both saline-treated controls and long-term exposed inserts. Thereby indicating an increased proliferative activity following acute exposure.

To compare responses between donors, the number of Ki67 positive cells and the γ-H2AX foci was normalized to the total number of DAPI positive nuclei(Figure 4B). Baseline levels differed between donors. For example, donor B38 displayed higher levels of both Ki67+ cells and γ-H2AX foci under control conditions. Despite this donor variance, the short-term exposure condition consistently showed increased proliferation and DNA damage across donors. In contrast, γ-H2AX levels in the long-term exposure condition were generally similar observed in control cultures. An exception was donor B22, where γ-H2AX foci were significantly in both the short and long-term exposure conditions compared to the control. Overall, acute BaP exposure induced the strongest DNA damage and proliferative responses while long-term exposure produced a more mild increase for these markers.

Comparison	Differentially Expressed Genes (Vulcano)	Top 5 Upstream Activators (DeCoupleR)	Top 5 Upstream Repressors (DeCoupleR)	Top Hallmark Pathways (GSEA)	Transcriptomic Profile & Trend	Biological Narrative & Interpretation
Short-term vs Control (Acute Exposure Phase)	-	DIDO1 ELF2 HSD17B8 GUCY1B1 ZFHX3	ZNF596 HMGA1 GREB1 NAB2 PAX3 TFAM	Cell cycle proliferation and metabolism (MYC targets v1) Oxidative Phosphorylation DNA repair Apical junctions Interferon responses	Acute cellular shock. Characterized by rapid transcriptional activation of immediate stress-response networks and early-stage metabolic adjustments to BaP exposure.	Reflects an acute transcriptional stress response of the AT2 cells to BaP exposure. Activation of HSD17B8, MYC-associated pathways, oxidative phosphorylation, and DNA repair programs suggest rapid metabolic adaptation and initiation of stress-responsive mechanisms(Andrade-Madrigal et al. 2026; Christmann et al. 2016; Lu et al. 2024). TFAM repression is consistent with mitochondrial stress and impaired mitochondrial homeostasis(Rong et al. 2021), indicating acute exposure challenges cellular energy homeostasis.
Long-term vs Control (Chronic Exposure Phase)	**Up:** *RAB3C* **Down:** *FOS* *OSR1*	CASP8AP2 TAF9B CAVIN1 FOXR2 ZSCAN5DP	ZNF746 ZNF837 HMGA1 ZNF596 ZNF224	Cell cycle progression Oxidative Phosphorylation DNA repair Apical junctions Interferon responses DNA Repair (Sustained Response) Epithelial Mesenchymal Transition E2F Targets Inflammatory Response	Sustained chronic cellular remodeling. Transition from acute stress to possible permanent phenotypic adaptation.	Indicates a transition toward chronic cellular adaptation. Sustained enrichment of DNA repair, inflammatory responses, and cell-cycle-associated pathways, together with activation of CASP8AP2, suggests persistent cellular damage and apoptotic signaling(Andrade-Madrigal et al. 2026; Catalanotto et al. 2024). Repression of HMGA1 and ZNF746 suggest long-term transcriptional adaptation and potential epithelial to mesenchymal remodeling(Xia et al. 2025).

Long-term vs Short-term (Adaptive / Transition Phase)	**Up:** *IFI27* **Down:** *WIF1* *FOS*	TFAM ZNF513 HMCES PAX3 TERF2	HSD17B8 CEBPZ GLI4 SUPT20H ZNF830	Cell cycle progression Oxidative Phosphorylation Apical junctions Interferon responses Oxidative Phosphorylation Epithelial Mesenchymal Transition	Demonstrates a possible shift where early acute responders are deactivated and long-term metabolic/mitochondrial repair mechanisms are recruited.	Reveals a transcriptional shift from acute injury responses towards a more adapted cellular state. Suppression of early stress response regulators, including HSD17B8, alongside activation of TFAM and oxidative phosphorylation pathways, suggest recruitment of mitochondrial repair mechanism and metabolic restoration mechanisms (Andrade-Madrigal et al. 2026; Lu et al. 2024; Rong et al. 2021). Downregulation of FOS further supports the reduced activation of the immediate stress response (Li et al. 2015).

Table 1: Transcription Factor comparisons and interpretations of the three different conditions.

Discussion

In this study, we developed and optimized a human primary alveolar air-liquid interface (ALI) model for air pollution toxicology studies. We subsequently applied this model to investigate the effects of acute and prolonged Benzo[a]Pyrene (BaP) exposure. We found that StemCell Medium (SCM) more effectively maintained alveolar organoid identity than alveolar organoid medium (AOM). These organoids were used to establish and optimize stable long-term ALI cultures. Acute and repeated BaP exposure induced distinct transcriptomic responses with repeated exposures being associated with pathway-level changes related to DNA repair, mitochondrial function, inflammatory signaling and epithelial remodeling. Furthermore, immunofluorescence staining following acute exposure confirmed increased proliferative activity and DNA damage, supporting the transcriptomic findings.

Maintaining a stable and enriched alveolar epithelial population is a critical prerequisite for generating representative ALI cultures. Therefore, we first evaluated the expansion of primary alveolar organoids and the influence of culture conditions on alveolar identity. Alveolar cells, used for our exposure studies, were isolated and cultured by optimization of existing protocols(Lamers et al. 2021),(Nikolic et al. 2017). During early passages in alveolar organoid medium (AOM), cultures consisted of a heterogeneous population of organoids, including both HT2-280+ alveolar organoids and TP63+ airway organoids. This observation may be related to a resemblance in supplements between both mediums(Sachs et al. 2019). Repeated HT2-280 based sorting was required to maintain an enriched alveolar population as the airway organoids seemed to take over the alveolar organoids. Previous reports showed that airway organoids may outcompete alveolar organoids during long-term expansion(Ebisudani et al. 2021).
Interestingly, TP63+ organoids re-emerged after sorting in several donors, indicating that alveolar identity was not fully maintained during prolonged culture. A recent study demonstrated that cultured AT2 cells can acquire KRT5+ and TP63+ phenotypes following interaction with fibrotic mesenchymal cells, highlighting the plasticity of alveolar epithelial cells(Kathiriya et al. 2022). Although the mechanism underlying the reappearance of the TP63+ organoids in our cultures remains unclear, these findings may indicate either expansion of residual airway-like cells or a loss of stable identity during culture.
Comparison of AOM with the SCM revealed no TP63+ organoids in the latter condition. These data suggest that the SCM more effectively preserves alveolar identity and reduces the emergence of airway-like populations. Therefore, despite a slower growth rate, the SCM appears to provide a more suitable platform for the long-term expansion of alveolar organoids intended for downstream ALI differentiation and exposure studies.

While alveolar organoids provide physiologically relevant *in vitro* models for studying distal lung biology and disease, their closed three-dimensional structure embedded in a matrix limits direct access to the apical surface and therefore restricts exposure to airborne toxicants. Furthermore, AT2 organoids generally maintain an AT2 phenotype, making it challenging to study the effect of air pollutants on AT1 cell populations, which represent the predominant epithelial population within the alveolus. To address these limitations, we established an ALI AT2/AT1 culture, enabling direct apical exposure while providing conditions that support epithelial differentiation.

The seeding density at the start of the ALI cultures influenced the morphology of the cells, with lower cell densities resulting in larger average cell areas. The phalloidin staining was used to measure the cell size, which was comparable to cells stained for the cell membrane marker ZO-1 as reported in literature despite the presence of the mixed AT1/AT2 population(Burgess et al. 2024). Moreover, TEER values obtained from the 100k and 200k seeding conditions were similar to previously reported alveolar ALI models, but did not seem to differ between conditions(Burgess et al. 2024). The TEER, however, decreased substantially under conditions that promote AT1 differentiation, which is consistent with reports that pre-differentiated AT1 plated cultures generally exhibit lower barrier resistance than AT2-dominated cultures(Burgess et al. 2024).

So far, most studies that use cell cultures to study exposure of pollutants rely on the use of tumor-derived or immortalized cell lines. While these models are highly reproducible and easy to maintain, they often display altered cellular signaling, transcriptional regulation, and metabolic activity compared to primary cells, which could limit the relevance for air pollutant toxicology studies(Suali et al. 2026). Therefore, we sought to increase the physiological relevance of the model by promoting transdifferentiation of human primary AT2 cells to AT1 cells. Several studies explored different factors to differentiate AT2 into AT1-like cells in organoids. These studies demonstrated that the withdrawal of AT2-promoting factors, such as EGF and Wnt agonists, combined with the addition of BMP4 or activation of YAP signaling, can drive differentiation towards an AT1-like phenotype(Burgess et al. 2024; Li et al. 2024; Ohnishi et al. 2024). Moreover, exposure to air could provide an additional boost in AT2 maturation and possible AT1 differentiation(Abo et al. 2022; Ghaedi et al. 2014). In our model, ALI culture combined with withdrawal of EGF and treatment of a LATS kinase-inhibitor resulted in morphological changes, a decrease in HT2-280 expression and a higher expression of the RAGE protein. However, the response to LATS kinase inhibitor varied substantially between donors.
Notably, substantial donor-to-donor variability was observed following LATS kinase-inhibitor treatment. While some donors displayed increased cell size(Burgess et al. 2024), enhanced RAGE expression and reduced HT2-280 positivity, others developed epithelial defects and detached from the insert within a time span of 2 weeks. The mechanisms underlying these differences remain unclear but may reflect inter-individual variation in epithelial plasticity, responsiveness to the YAP pathway activation, or the ability to maintain epithelial integrity during differentiation. Additionally, reactivity towards the compounds was previously tested in 3D grown alveolar organoids and could therefore differ for 2D grown cells(Fontoura et al. 2020). Taken together, these findings suggest that although LATS-in-1 promotes features associated with AT1 differentiation, the resulting loss of culture stability limits the applicability for long-term exposure studies.

Comparison of the transcriptomic profiles between the cultures at week 1 after ALI and 5 weeks at ALI revealed substantial differences in cellular identity. Deconvolution analysis, based on AT1- and AT2-associated genes, demonstrated an overall reduction in both AT1 and AT2 identities across donors over time, although some donor-specific variation in AT1 signatures was observed. In contrast, expression of the transitional state markers increases over time for one donor and remained relatively stable for the others. While these findings should be interpreted with caution, as deconvolution estimates are based on bulk RNA sequencing data rather than direct cell identification such as single cell captures, they suggest that prolonged ALI cultures results in significant transcriptional remodeling of the alveolar epithelium.

Consistent with this observation, RNA sequencing revealed a downregulation of genes involved in cell cycle progression, including regulators of mitosis and proliferation. In addition, the GSEA displayed increased EMT and inflammatory signaling pathways were upregulated. Together, these findings suggest a gradual loss of classical AT1 and AT2 transcriptional signatures and a shift towards an altered epithelial state during prolonged ALI culture. Although similar long-term transcriptional changes have not been reported for alveolar ALI cultures, they may reflect ongoing epithelial adaptation during prolonged culture. Furthermore, RNAseq revealed a downregulation of mucosal epithelial keratins *KRT4* and *KRT13*, markers of hillock cells(Hewitt and Lloyd 2021), suggests the cells are shifting away from a stratified or squamous lineage toward a more stable, polarized monolayer.
Interestingly, we observed similar plasticity in our organoid cultures, where airway-like populations re-emerged during prolonged culture. This observation is consistent with previous reports describing a shift towards basal-like cell populations in organoid cultures grown in commercial medium or in the presence of mesenchymal cells, further supporting that the alveolar identity remains highly plastic under various culture conditions(Kathiriya et al. 2022).
Therefore, future studies should investigate how prolonged ALI culture affects alveolar lineage stability overtime.

Most studies investigating the exposure of lung cells to agents such as BaP, have used submerged immortalized cell lines(Boule et al. 2025), despite the knowledge that cells react in different ways when exposed to particulate matter submerged or via aerosolized particles(Allouche et al. 2025; Boule et al. 2025; Cappellini et al. 2020). Nebulization is therefore considered a more physiologically relevant exposure method because it better mimics inhalation and avoids interactions between compounds and the culture medium. Using this approach, exposure of the primary alveolar ALI cultures to nebulized BaP induced distinct pathway-level response despite having relatively few significantly differentially expressed genes (DEGs). The limited number of DEGs may partially be explained by the selected sampling time point. Cells were harvested 24 hours after the final exposure, whereas several canonical BaP responsive genes, like CYP1A1, are known to peak much earlier following exposure(Allouche et al. 2025; Boule et al. 2025). These studies have reported substantially higher CYP1A1 expression 6 hours after exposure compared to the 24 hours, suggesting that transient responses may have been missed in the current experimental design.

One of the findings across the exposure conditions was the upregulation of DNA repair pathways. This observation is in line with previous studies demonstrating activation of DNA repair mechanisms following exposure to BaP metabolites(Christmann et al. 2016). Activation of these repair genes could harness an protective effect for following up exposure at the costs of DNA mutations. As BaP metabolism generates reactive intermediates capable of inducing DNA adducts and oxidative damages, activation of repair pathways likely represent an adaptive protective response.
Interestingly, long-term exposed cultures exhibited fewer γH2AX+ foci compared to the short-term exposed cultures. this may indicate that repeated exposure enhances the capacity of the cells to recognize and repair the DNA damage. While such adaptation could provide protection against repeated exposures, prolonged activation of these repair mechanisms may also increase the likelihood of introducing mutations, potentially contributing to carcinogenic outcomes(Christmann et al. 2016).

The upstream regulator analysis further provided additional insight into the potential transcriptional programs underlying these responses. Long-term exposure compared to short-term exposure resulted in increased predicted activity of TFAM and HMCES, which are involved in mitochondrial genome maintenance and DNA repair, respectively(Rong et al. 2021; Srivastava et al. 2020). Although both the DeCoupleR and GSEA analyses were derived from the same RNA seq dataset, they converged on similar biological processes involving the DNA damage repair and metabolic maintenance. Together, these analyses suggest that repeated BaP exposure is associated with adaptive stress-response programs aimed at maintaining mitochondrial function and genomic stability to counteract prolonged chemical insult. Relatively few genes met the threshold for DEG, indicating that transcriptional response may be distributed across multiple genes with relatively small expression changes, becoming more apparent at the pathway level than at individual gene level.

In contrast, short-term exposure was characterized by increased predicted activity of DIDO1, ELF2 and HSD17B8, supporting activation of an immediate cellular stress-response related to cell proliferation changes, metabolism changes, chromatin remodeling and apoptosis programs, following acute BaP exposure(Garcia-Domingo et al. 2003; Guan et al. 2017; Lu et al. 2024). Prolonged exposure additionally increased the activity of CASP8AP2 and TAF9B, suggesting altered regulation of apoptotic and transcriptional response pathways(Catalanotto et al. 2024; Pan et al. 2019). Combined, these findings indicate a shift from an acute stress-response phenotype towards a more adaptive long-term exposure state.

In addition to DNA repair, oxidative phosphorylation pathways were significantly enriched in both short and long-term exposure conditions. Similar pathways were reported following chronic low dose BaP exposure in aquatic toxicology models(Zeb et al. 2024). Another study to bronchial exposed models exhibited a downregulation of oxidative involved gene HMOX1 after 24h exposure and undetectable levels after 4 weeks of repeated low dose exposures(Cervena et al. 2019). Combined, these observations suggest that possible mitochondrial adaptations are an important component of the cellular response to BaP exposure to ensure a prolonged exposure does not interfere with the organism.

Although pathway level alterations were more pronounced than individual gene changes, several genes may provide insight into the biological processes occurring during prolonged exposure.
FOS expression was consistently reduced in long-term exposed cultures compared to both control and short exposure groups. Normally the expression of immediate early response proto-oncogene FOS, influences the role of the proliferation of the cells and it has been seen to increase its expression in rats when exposed to PM2.5(Li et al. 2015). Its downregulation may indicate a transition from an acute stress response toward a more adapted cellular state. Interestingly, GSEA analysis and Ki67 immunostaining suggested increased proliferative activity despite reduced *FOS* expression, implying that alternative signaling pathways may drive proliferation in these cultures. Potential candidates include c-Jun activation through PI-3K/Akt/ERK associated pathways(Jiao et al. 2008).

RAB3C expression levels were increased following prolonged exposure. As *RAB3C* regulates intracellular vesicle trafficking and exocytosis, its upregulation may reflect cellular adaptation mechanisms aimed at maintaining intercellular communication as response to chronic adaptation(Chang et al. 2023). In addition, *IFI27* was upregulated in the long-term compared to the short-term exposed conditions, but little is known currently regarding the relationship between *IFI27* and BaP exposure. Normally the gene acts is associated with interferon signaling, apoptosis, and cellular stress responses, making is a plausible contributor to the inflammatory signatures observed in the pathways(Shojaei and McLean 2025). Moreover, the decreased predicted activity of HSD17B8 and CEBPZ in the long-term exposure compared to the short-term condition may indicate attenuation of acute stress-response signaling and broader changes in transcriptional regulation as cells transition towards a chronic adaptation phenotype(Lu et al. 2024; Shaowen Cheng 2023).

Contrasting previous studies reporting activation of cytokine signaling together with alteration in the extracellular matrix organization and remodeling after BaP exposure in submerged bronchial epithelial cell lines(Andrade-Madrigal et al. 2026). We found a upregulation in epithelial to mesenchymal transition (EMT) in the long-term exposed cells, while a downregulation was found in the short-term exposure. HMGA1, one of the downregulated upstream transcription factors, was previously found to drive EMT in obliterative bronchiolitis(Xia et al. 2025). Similarly, the interferon responses were upregulated in the long-term exposed cells while downregulated in the short-term exposed cells. This suggests that prolonged exposure induces a distinct transcriptional state that differs from the immediate response observed after a single exposure event.
The observed upregulation of interferon signaling together with EMT pathways may indicate the development of a chronic adaption phenotype characterized by increased inflammatory signaling and epithelial remodeling. This interpretation is supported by the contrast between short and long-term exposures, where repeated exposure was associated with more pronounced immune-related responses.

A strength of the present study is the use of primary alveolar cells isolated form pediatric donors, all younger than 6 years of age without a smoking history. This minimizes potential confounding effects associated with prior exposure to cigarette smoke, which is known to induce persistent transcriptional, epigenetic, and inflammatory alterations in the lung epithelium(Liu et al. 2010; van der Does et al. 2022). Consequently, the observed responses are likely to reflect the effects of the experimental BaP exposures rather than pre-existing smoking related adaptations. However, the exclusive use of pediatric donor may also limit the generalizability of the findings to adult populations, particularly individuals with a history of smoking of chronic environmental exposures(Eenjes et al. 2021).

Collectively, our data demonstrate that human primary alveolar cells are physiologically relevant to model airborne pollutant exposure and our studies highlight the importance of chronic exposure models for studying the impact of air pollutants. Interestingly, our findings suggest that chronic BaP exposure of primary alveolar cells does not simply prolong the effects of acute exposure, but instead induces a distinct adaptive transcriptional program characterized by enhanced DNA repair, altered mitochondrial activity, inflammatory signaling and epithelial remodeling. This suggests that chronic exposure brings alveolar cells in a primed immunological state.

This could have clinical implications as people living in polluted areas may be more vulnerable and at higher risk to additional triggers.

Material and methods

Patient material

Tumor-free human lung tissue was obtained from resection material at the Erasmus Medical Center in Rotterdam, The Netherlands. The resected material originates from disease-free part of resected lung lobe from patients with lung tumors, congenital pulmonary airway malformation (CPAM) or congenital lobar overinflation (CLO). All obtained lung samples were used anonymously and with informed consent following the "Human Tissue and Medical Research: Code of conduct for responsible use (2011, www.federa.org)" guidelines. Obtaining the material was approved by the Medical Ethical Committee (METC nr. MEC-2017-302). The cells used in the ALI alveolar exposure cultures were donors below the age of three years old. Donor characteristics used in this research are in supplementary table 2.

Isolation of alveolar type 2 cells

All key resources are provided in supplementary table 3. Primary alveolar type 2 cells were isolated as described(Lamers et al. 2021). Briefly, human lung tissue was manually disrupted to very small pieces. The pieces were digested with TrypLE (Gibco, cat no. 12604013) followed by mechanically disrupting and vortexing the sample. Advanced DMEM/F12 medium (ThermoFisher, cat. no 12634–010) was added and the suspension was strained over a 100 µm strainer (Falcon, Corning, cat. no 352360). The cells were treated with red blood cell (RBC) lysis buffer (Sigma, Roche, cat. no 11814389001) until the pellet appeared white and the cells were washed several times with Advanced DMEM/F12 medium. Subsequently, the cells were seeded in 30 µL BME drops (Trevigen, cat no. 3533-010-02) and solidified in the incubator at 37 ºC for 15 min before adding the PneumaCult alveolar plating medium (StemCell, cat. no 100-0847) or complete human alveolar organoid medium (Supplementary Table 4-5). Medium was changed twice per week.

Culturing organoids

Organoids were recovered from the BME by washing with cold 1% bovine serum albumin (BSA) in DPBS, and digested using TrypLE. The medium was aspirated and the pellet was resuspended in Soy Bean Trypsin Inhibitor (SBTI). The cells were resuspended in SCM after centrifugation. Cell number and viability were determined and cells were seeded in 30 µL BME at a density of 10.000 cells per drop. The drops were solidified in an incubator for 15 min and PneumaCult alveolar seeding medium was added.

Purification of alveolar type 2 cells

FACS sorting was performed when the organoids were fully grown (4 weeks). The sorting and growth works best when there are around 125k cells per drop. It can be that the cells need one passage before reaching this stage. In short, the cells were made single cell, dissolved in 1 mL of FACS buffer (2.5% BSA, 2 mM EDTA in DPBS) containing 5 µM of RI (Abmole, cat no. Y-27632) and counted. A unstained population of 100k cells was set aside. The rest of the cell suspension was resuspended in FACS buffer with primary antibody HTII-280 at 1:40 dilution. For 1×10^6 cells, 5 µL antibody (stock concentration) was added. The solution was incubated turning for 20-25 min in a cold room. We centrifuged cells at 400 × g for 3 min, and the secondary antibody Alexa Fluor ®488 Donkey anti Mouse IgG at 1:400 dilution in FACS buffer was added. The solution was incubated at 4°C

turning for 15 minutes. FACS buffer was added to the solution and spun down at 400 × g. The cells were washed once in 2 mL FACS buffer, centrifuged, and resuspended in 0.5 mL FACS buffer with 5 µM of RI. The cells were placed in a FACS tube with 70 µM filter and sorted for HT2-280+ (AF-488). Once sorted, the cells were resuspended in BME to a concentration of 20k cells per 30 µL and medium was added.

ALI culture setup

The schematic overview of the co-culture setup is shown in supplementary figure 2A. Briefly, the basolateral side of the 24 well inserts (Costar, Corning, cat no. 3470) was coated using co-culture coating solution (30 µg/mL PureCol, 10 µg/mL Human Fibronectin, 10 µg/mL BSA in 1 × DPBS) overnight (ON) at 37 ºC. The next day, excess coating solution was removed and the inserts were dried upside down in a cell culture hood for 2-3 hours. Human microvascular endothelial cells (hMVECs) were trypsinized with TE buffer and $6.7*10^4$ cells were seeded on the basolateral side of an insert membrane in 50 µL EGM-2MV (Lonza, cat no. CC-3202) and allowed to attach to the membrane for 3.5-4 hours, after which EGM-2MV was added. After 3-4 days $1,5*10^5/cm^2$ alveolar cells were seeded on the apical side in medium consisting of SAGM with 2% FCS:EGM-2MV in a 2:1 combination with 5 µM of RI, after which a live cell count was executed. We plated $150k/cm^2$ alveolar cells unless stated otherwise. After 3 days the cells were put to ALI and the cells were differentiated for 1 week (unless stated otherwise) before being used for exposure experiments.

During AT2 to AT1 differentiation experiments other small molecules or morphogens, like LATS-in-1 and BMP4, were added to the basolateral medium for the complete duration of the experiment.

Trans-epithelial electrical resistance

To measure the electrical resistance, 500 µL of DPBS with Mg^{2+} and Ca^{2+} was added to the apical compartment of the inserts. The inserts were placed back into the incubator for 5 min. The STX2 electrode (World precision Instruments) was connected to the EVOM2. The electrode was placed into the prewarmed well and the resistance measurement was taken. The resistance measurements were corrected for the surface area of the insert.

Nebulization of air pollutants

ALI cultures were nebulized according to the manufacturer's instructions. Briefly, the inserts were washed with PBS plus Mg^{2+} and Ca^{2+} and placed into the chamber of the Vitrocell Cloud-α system. The chamber was primed with 200 µL of 0.9% saline, whereafter the air pollutant was added in 200 µL and nebulized. Subsequently, another 200 µL of saline was nebulized to flush most of the air pollutants out. For the control exposures, 200 µL of 0.9% saline was nebulized. Benzo[a]pyrene (BaP) was dissolved to 5.8 µM in 0.9% saline to meet regulatory requirements. For the long-term exposures, the inserts were exposed twice a week for 4 weeks with 200 µL of 0,725 µM BaP. The day after the last exposure the cultures were harvested following a PBS plus Mg^{2+} and Ca^{2+} wash.

RT-qPCR

Mono and co-cultures were washed with PBS before starting the RNA isolation. For the co-cultures, RLT lysis buffer from the RNeasy kit (QAIGEN, cat. 74106) was added on top of the insert, while the inserts of the mono AT2 cultures were excised and added in a RLT lysis buffer. Total RNA was isolated following the QAIGEN

protocol and eluted in 30 µL ddH_2O. RNA concentration was measured using the NanoDrop™ 2000 (Thermo Scientific, ND-2000). One µg of isolated RNA was converted to cDNA with the iScript™ cDNA Synthesis Kit (BioRad, cat. 1708891). Subsequent qPCR was performed using Platinum Taq (Invitrogen, cat. 10966034) with SybrGreen (Sigma, cat. S9430) in a CFX96 Touch Real-Time PCR Detection System. qPCR primers can be found in supplementary table 6. The PCR program was set to 95°C for 5 min, followed by 40 cycles of 95°C for 30 sec, 60°C 1 min, 72°C 30 sec, plate read 72°C 10 min, melting curve 50-95°C read every 0.5°C 3 min. Excel was used to normalize the data to *GAPDH* as internal standard. Fold increases to the control were used to compare expression between groups. The data was displayed using GraphPad Prism 11.0.2.

RNA bulk seq

RNA bulk seq was performed by isolating RNA from the cultures as described and 300 ng of RNA was used for the RNA seq (Plasmidsaurus). The raw data was analyzed using Rstudio (version: 2026.01.1+403 and differential expressed gene (DEG) analysis was performed with DESeq2 package (version 1.50.2). Other packages used in the analysis were AnnotationDbi (version 1.72.0), org.Hs.eg.db (version 3.22.0). The heatmaps were made with package pheatmap (version 1.0.13) and plotted with ggplot2 (version 4.0.2), ggrepel (version 0.9.7) and dplyr (version 1.2.0). Benjamini–Hochberg correction was applied to p-value significant genes.
Gene Set Enrichment Analysis (GSEA) was performed using fgsea (version 1.36.2) and the top 20 pathways were plotted as a normalized expression score (NES) in a heatmap that includes the gene count and p_adjvalue.
DecoupleR (version 2.17.0) was used to extract possible transcription factor activity.

Immunofluorescence (IF)

Organoids

Organoids were cultured in a black flat bottom 96-well plate (Corning, Falcon, cat no 353219), fixated with 4% paraformaldehyde (PFA) and processed for whole mount immunostaining as previously described by van Horik et al(van Horik et al. 2026). Primary and secondary antibodies with dilution can be found in Supplementary table 7. Images were taken using the SP-5 Leica confocal. Images were processed with ImageJ.

Inserts

The co-cultures and mono-cultures were washed with DPBS plus Mg^{2+} and Ca^{2+}, cut from the insert and fixated in PFA 4% at RT for 20 min and washed trice with PBS. Subsequently, the staining was performed as stated previously(Iriondo et al. 2025). The modifications are stated as follows, the cut membranes were blocked with 1% (w/v) BSA and 5% (v/v) normal donkey serum in 0.1% PBS-T at RT for 1 h. Primary antibodies (Supplementary Table 7) were diluted in blocking buffer and incubated on the membranes overnight at 4 °C. Following day, the membranes were washed with 0.03% (v/v) PBS-T and incubated with secondary antibodies (Supplementary Table 7), phalloidin (Fisher Scientific, cat. no. 14879680) and 1:2000 DAPI solution for 2 hours in the dark after being rinsed and washed thrice with 0.03% (v/v) PBS-T. The membranes were mounted on slides and fluorescent images were taken with ECHO Revolve and confocal images using the SP-5 Leica confocal. Images were processed with ImageJ version 1.16.0-1.54t.

Analyzing projected cell area

Alveolar inserts were cultured at various cell seeding densities and subsequently stained for phalloidin and DAPI. Fluorescent pictures were acquired, and nuclei were segmented from the DAPI channel by generating a binary mask (Supplementary Material 1). Cell segmentation was performed using the marker-controlled watershed function from the MorphoLibJ plugin, using the DAPI-derived nuclei masks as markers and the phalloidin signal to define cell boundaries(Legland et al. 2016) (Supplementary Material 2). Individual cell areas were further quantified using a custom Fiji/imageJ script (Supplementary Material 3). The resulting measurements were further analyzed with Excel and GraphPad Prism.

Counting DAPI/KI67/γ-H2AX foci

Exposed insert membranes were previously stained for KI67, γ-H2AX and DAPI. DAPI positive nuclei and Ki67+ cells were quantified using Fiji scripts (Supplementary Materials 4 & 5). γ-H2AX foci were quantified manually in ImageJ by adjusting the image contrast and using the "Cell counter" plugin. For each membrane, 3-4 individual fields of view were analyzed. The number of Ki67+ cells was normalized to the total number of DAPI positive nuclei. Similarly, the number of γ-H2AX foci spots was normalized to the total number of DAPI positive nuclei.

Statistical analysis

Data in graphs is represented as means with a standard error. The graphs were made using Graphpad Prism version 11. Statistical differences between conditions were assessed with a one way ANOVA and the analysis performed using Graphpad. P values below 0.05 are considered significant.

ACKNOWLEDGEMENT

The authors would like to thank Prof. Irwin Reiss for his contributing (in part) the Vitrocell Cloud-α system. The authors are supported by Convergence, the alliance between Erasmus Medical Center Rotterdam, Erasmus University Rotterdam and Delft University of Technology, and are part of the convergence flagship "Decoding Real-Time, Personalized Health Impact of Climate Change and Pollution".

FUNDING

S.K. was supported by The Erasmus MC-Erasmus University-TU-Delft Flagship ("Decoding Real-Time, Personalized Health Impact of Climate Change and Pollution"). The schematic overviews in each figure were made with Biorender: Koornneef, S. (2026)

STATEMENTS AND DECLARATIONS

The authors declare that the research was conducted in the absence of any commercial or financial relationships that could be construed as potential conflicts of interest.

AUTHOR CONTRIBUTIONS:

Conceptualization: SK, RJR

Methodology: SK, CIM, JZ, MBvK, ABdM, HBT, JMS, RJR

Investigation: SK, CIM MBvK, ABdM, RJR

Formal analysis: SK, MBvK, ABdM, RJR

Data curation: SK, RJR

Visualization: SK, MBvK, ABdM, RJR

Validation: SK, MBvK, ABdM, RJR

Supervision: RJR

Funding acquisition: RJR

Project administration: SK, RJR

Writing—original draft: SK, RJR

Writing—review & editing: SK, CIM, JZ, MBvK, ABdM, HBT, JMS, RJR

AVAILABILITY OF DATA AND MATERIALS

The datasets used and/or analysed during the current study are available from the corresponding author on reasonable request.

ETHICS APPROVAL

The human study was reviewed and approved by the Daily Board of the Medical Ethics Committee (METC) of Erasmus MC Rotterdam, The Netherlands (MEC-2017-302).

References

(HEI) HEI (2025) State of Global Air 2025: A Report on Air Pollution and Its Role in the World's Leading Causes of Death.

(WHO) WHO (2021) WHO global air quality guidelines: Particulate matter ($PM_{2.5}$ and PM_{10}), ozone, nitrogen dioxide, sulfur dioxide and carbon monoxide. World Health Organization, Geneva, Switzerland

Abo KM, Sainz de Aja J, Lindstrom-Vautrin J, et al. (2022) Air-liquid interface culture promotes maturation and allows environmental exposure of pluripotent stem cell-derived alveolar epithelium. JCI Insight 7(6) doi:10.1172/jci.insight.155589

Allouche Y, Marchetti S, Bengalli R, et al. (2025) Comparison of submerged and air liquid interface exposure: limitations and differences in the toxicological effects evaluated in bronchial epithelial cells. Environ Res 279(Pt 2):121856 doi:10.1016/j.envres.2025.121856

Andrade-Madrigal C, Rojas-Fuentes C, Diaz-Mijares J, et al. (2026) Modeling Chronic BaP Exposure in Bronchial Epithelial Cells Reveals Multi-Scale Drivers of Early Preneoplastic Reprogramming. Cells 15(6) doi:10.3390/cells15060566

Boule S, Verhaeghe L, Courcot D, Landkocz Y (2025) Comparison of the behavior of human lung epithelial cell lines cultured at the air-liquid interface and assessment of their responses after benzo(a)pyrene exposure. Toxicol In Vitro 109:106122 doi:10.1016/j.tiv.2025.106122

Bukowska B, Mokra K, Michalowicz J (2022) Benzo[a]pyrene-Environmental Occurrence, Human Exposure, and Mechanisms of Toxicity. Int J Mol Sci 23(11) doi:10.3390/ijms23116348

Burgess CL, Huang J, Bawa PS, et al. (2024) Generation of human alveolar epithelial type I cells from pluripotent stem cells. Cell Stem Cell 31(5):657-675 e8 doi:10.1016/j.stem.2024.03.017

Cappellini F, Di Bucchianico S, Karri V, et al. (2020) Dry Generation of CeO(2) Nanoparticles and Deposition onto a Co-Culture of A549 and THP-1 Cells in Air-Liquid Interface-Dosimetry Considerations and Comparison to Submerged Exposure. Nanomaterials (Basel) 10(4) doi:10.3390/nano10040618

Catalanotto M, Vaz JM, Abshire C, et al. (2024) Dual role of CASP8AP2/FLASH in regulating epithelial-to-mesenchymal transition plasticity (EMP). Transl Oncol 39:101837 doi:10.1016/j.tranon.2023.101837

Cervena T, Vrbova K, Rossnerova A, Topinka J, Rossner P, Jr. (2019) Short-term and Long-term Exposure of the MucilAir Model to Polycyclic Aromatic Hydrocarbons. Altern Lab Anim 47(1):9-18 doi:10.1177/0261192919841484

Chang YC, Li CH, Chan MH, et al. (2023) Overexpression of synaptic vesicle protein Rab GTPase 3C promotes vesicular exocytosis and drug resistance in colorectal cancer cells. Mol Oncol 17(3):422-444 doi:10.1002/1878-0261.13378

Chen P, Li Y, Zhang Y, Xue C, Hopke PK, Li X (2023) Dynamic Changes of Composition of Particulate Matter Emissions during Residential Biomass Combustion. Environmental Science & Technology 57(40):15193-15202 doi:10.1021/acs.est.3c05412

Christmann M, Boisseau C, Kitzinger R, et al. (2016) Adaptive upregulation of DNA repair genes following benzo(a)pyrene diol epoxide protects against cell death at the expense of mutations. Nucleic Acids Res 44(22):10727-10743 doi:10.1093/nar/gkw873

Daum N, Kuehn A, Hein S, Schaefer UF, Huwer H, Lehr CM (2012) Isolation, cultivation, and application of human alveolar epithelial cells. Methods Mol Biol 806:31-42 doi:10.1007/978-1-61779-367-7_3

Ebisudani T, Sugimoto S, Haga K, et al. (2021) Direct derivation of human alveolospheres for SARS-CoV-2 infection modeling and drug screening. Cell Rep 35(10):109218 doi:10.1016/j.celrep.2021.109218

Eenjes E, van Riet S, Kroon AA, et al. (2021) Disease modeling following organoid-based expansion of airway epithelial cells. Am J Physiol Lung Cell Mol Physiol 321(4):L775-L786 doi:10.1152/ajplung.00234.2020

Fontoura JC, Viezzer C, Dos Santos FG, et al. (2020) Comparison of 2D and 3D cell culture models for cell growth, gene expression and drug resistance. Mater Sci Eng C Mater Biol Appl 107:110264 doi:10.1016/j.msec.2019.110264

Garcia-Domingo D, Ramirez D, Gonzalez de Buitrago G, Martinez AC (2003) Death inducer-obliterator 1 triggers apoptosis after nuclear translocation and caspase upregulation. Mol Cell Biol 23(9):3216-25 doi:10.1128/MCB.23.9.3216-3225.2003

Ghaedi M, Mendez JJ, Bove PF, Sivarapatna A, Raredon MS, Niklason LE (2014) Alveolar epithelial differentiation of human induced pluripotent stem cells in a rotating bioreactor. Biomaterials 35(2):699-710 doi:10.1016/j.biomaterials.2013.10.018

Grytting VS, Skuland T, Ballangby J, et al. (2024) The effects of fine particulate matter (SRM 2786) on three different 3D lung models exposed at the air-liquid interface - A comparative study. Toxicol In Vitro 98:105841 doi:10.1016/j.tiv.2024.105841

Guan FH, Bailey CG, Metierre C, et al. (2017) The antiproliferative ELF2 isoform, ELF2B, induces apoptosis in vitro and perturbs early lymphocytic development in vivo. J Hematol Oncol 10(1):75 doi:10.1186/s13045-017-0446-7

Hewitt RJ, Lloyd CM (2021) Regulation of immune responses by the airway epithelial cell landscape. Nat Rev Immunol 21(6):347-362 doi:10.1038/s41577-020-00477-9

Huang Y, Wang J, Huang S, Zhang X, Hu J (2023) 5-Lipoxygenase Contributes to Benzo[a]pyrene-Induced Cytotoxicity and DNA Damage in Human Bronchial Epithelial Cells. Int J Toxicol 42(2):172-181 doi:10.1177/10915818221146286

Iriondo C, Koornneef S, Skarp KP, Buscop-van Kempen M, Boerema-de Munck A, Rottier RJ (2024) Simple-Flow: A 3D-Printed Multiwell Flow Plate to Coculture Primary Human Lung Cells at the Air-Liquid Interface. ACS Biomater Sci Eng doi:10.1021/acsbiomaterials.4c01322

Iriondo C, Koornneef S, Skarp KP, Buscop-van Kempen M, Boerema-de Munck A, Rottier RJ (2025) Protocols to co-culture human primary lung cells in the simple-flow device. STAR Protoc 6(3):103892 doi:10.1016/j.xpro.2025.103892

Jiao S, Liu B, Gao A, et al. (2008) Benzo(a)pyrene-caused increased G1-S transition requires the activation of c-Jun through p53-dependent PI-3K/Akt/ERK pathway in human embryo lung fibroblasts. Toxicol Lett 178(3):167-75 doi:10.1016/j.toxlet.2008.03.012

Kathiriya JJ, Wang C, Zhou M, et al. (2022) Human alveolar type 2 epithelium transdifferentiates into metaplastic KRT5(+) basal cells. Nat Cell Biol 24(1):10-23 doi:10.1038/s41556-021-00809-4

Koornneef S, Horne FJ, Thio HB, et al. (2025) Advances in organ-on-a-chip technology to examine the impact of air pollutants on epithelial barrier tissues. Environ Res 285(Pt 1):122289 doi:10.1016/j.envres.2025.122289

Lamers MM, van der Vaart J, Knoops K, et al. (2021) An organoid-derived bronchioalveolar model for SARS-CoV-2 infection of human alveolar type II-like cells. EMBO J 40(5):e105912 doi:10.15252/embj.2020105912

Legland D, Arganda-Carreras I, Andrey P (2016) MorphoLibJ: integrated library and plugins for mathematical morphology with ImageJ. Bioinformatics 32(22):3532-3534 doi:10.1093/bioinformatics/btw413

Li R, Kou X, Xie L, Cheng F, Geng H (2015) Effects of ambient PM2.5 on pathological injury, inflammation, oxidative stress, metabolic enzyme activity, and expression of c-fos and c-jun in lungs of rats. Environ Sci Pollut Res Int 22(24):20167-76 doi:10.1007/s11356-015-5222-z

Li Y, Prakash YS, Tan Q, Tschumperlin D (2024) Defining signals that promote human alveolar type I differentiation. Am J Physiol Lung Cell Mol Physiol 326(4):L409-L418 doi:10.1152/ajplung.00191.2023

Lin KC, Yen CZ, Yang JW, Chung JHY, Chen GY (2022) Airborne toxicological assessment: The potential of lung-on-a-chip as an alternative to animal testing. Materials Today Advances 14:100216 doi:10.1016/j.mtadv.2022.100216

Liu F, Killian JK, Yang M, et al. (2010) Epigenomic alterations and gene expression profiles in respiratory epithelia exposed to cigarette smoke condensate. Oncogene 29(25):3650-64 doi:10.1038/onc.2010.129

Lu YS, Chen J, He XR, et al. (2024) Perfluorooctane sulfonate (PFOS) and benzo[a]pyrene (BaP) synergistically induce neurotoxicity in C6 rat glioma cells via the activation of neurotransmitter and Cyp1a1-mediated steroid hormone synthesis pathways. Food Chem Toxicol 193:115058 doi:10.1016/j.fct.2024.115058

M. Ochs HOB (2019) The Structural and Physiologic Basis of Respiratory Disease. Kendig's Disorders of the Respiratory Tract in Children:63-100.e2 doi:10.1016/B978-0-323-44887-1.00006-7

Nikolic MZ, Caritg O, Jeng Q, et al. (2017) Human embryonic lung epithelial tips are multipotent progenitors that can be expanded in vitro as long-term self-renewing organoids. Elife 6 doi:10.7554/eLife.26575

Ohnishi Y, Masui A, Suezawa T, et al. (2024) Screening of factors inducing alveolar type 1 epithelial cells using human pluripotent stem cells. Stem Cell Reports 19(4):529-544 doi:10.1016/j.stemcr.2024.02.009

Olesiejuk K, Chalubinski M (2023) How does particulate air pollution affect barrier functions and inflammatory activity of lung vascular endothelium? Allergy 78(3):629-638 doi:10.1111/all.15630

Pan JA, Tang Y, Yu JY, et al. (2019) miR-146a attenuates apoptosis and modulates autophagy by targeting TAF9b/P53 pathway in doxorubicin-induced cardiotoxicity. Cell Death Dis 10(9):668 doi:10.1038/s41419-019-1901-x

Rong Z, Tu P, Xu P, et al. (2021) The Mitochondrial Response to DNA Damage. Front Cell Dev Biol 9:669379 doi:10.3389/fcell.2021.669379

Ryu Y, Roh S, Joung YS (2023) Assessing the cytotoxicity of aerosolized carbon black and benzo[a]pyrene with controlled physical and chemical properties on human lung epithelial cells. Sci Rep 13(1):9358 doi:10.1038/s41598-023-35586-7

Sachs N, Papaspyropoulos A, Zomer-van Ommen DD, et al. (2019) Long-term expanding human airway organoids for disease modeling. EMBO J 38(4) doi:10.15252/embj.2018100300

Sengupta A, Dorn A, Jamshidi M, et al. (2023) A multiplex inhalation platform to model in situ like aerosol delivery in a breathing lung-on-chip. Front Pharmacol 14:1114739 doi:10.3389/fphar.2023.1114739

Shaowen Cheng JY, Yudie Wang, Lina Xian, Zhihua Hu, Lingyun Zou (2023) The function and regulation of CCAAT/enhancer binding protein ε. European Journal of Inflammation 21 doi:10.1177/1721727X231153322

Shojaei M, McLean AS (2025) Interferon-stimulated gene IFI27 as a multifaceted candidate target in precision medicine. Trends Immunol 46(3):219-228 doi:10.1016/j.it.2025.01.008

Srivastava M, Su D, Zhang H, et al. (2020) HMCES safeguards replication from oxidative stress and ensures error-free repair. EMBO Rep 21(6):e49123 doi:10.15252/embr.201949123

Suali L, Chia Y, Rustin C, et al. (2026) Primary cell cultures versus immortalized cell lines: critical comparative insights into biological fidelity and translational applications. Biotech Histochem 101(7):429-455 doi:10.1080/10520295.2026.2714776

van der Does AM, Mahbub RM, Ninaber DK, et al. (2022) Early transcriptional responses of bronchial epithelial cells to whole cigarette smoke mirror those of in-vivo exposed human bronchial mucosa. Respir Res 23(1):227 doi:10.1186/s12931-022-02150-2

van Donkelaar A, Martin RV, Li C, Burnett RT (2019) Regional Estimates of Chemical Composition of Fine Particulate Matter Using a Combined Geoscience-Statistical Method with Information from Satellites, Models, and Monitors. Environ Sci Technol 53(5):2595-2611 doi:10.1021/acs.est.8b06392

van Horik C, Benthem F, Buscop-van Kempen M, et al. (2026) Activating KRAS mutations mark premalignant cystic structures in congenital pulmonary airway malformations. Respir Res 27(1):56 doi:10.1186/s12931-025-03491-4

Wang Y, Zhai W, Wang H, Xia X, Zhang C (2015) Benzo(a)pyrene promotes A549 cell migration and invasion through up-regulating Twist. Arch Toxicol 89(3):451-8 doi:10.1007/s00204-014-1269-8

Whitsett JA, Kalin TV, Xu Y, Kalinichenko VV (2019) Building and Regenerating the Lung Cell by Cell. Physiol Rev 99(1):513-554 doi:10.1152/physrev.00001.2018

Xia T, Hou Z, Wang S, et al. (2025) HMGA1 drives EMT in obliterative bronchiolitis through epigenetic regulation of chromatin accessibility in pulmonary epithelial cells. Clin Epigenetics 17(1):192 doi:10.1186/s13148-025-02000-0

Yang Z, Zhang Y, Ran S, et al. (2025) Exposure to ambient air pollution over developmental stages induced neurodevelopmental impairment in mice offspring via microbiome-gut-brain axis. Part Fibre Toxicol 22(1):20 doi:10.1186/s12989-025-00637-6

Zeb R, Yin X, Chen F, Wang KJ (2024) Chronic exposure to environmental concentrations of benzo[a]pyrene causes multifaceted toxic effects of developmental compromise, redox imbalance, and modulated transcriptional profiles in the early life stages of marine medaka (Oryzias melastigma). Aquat Toxicol 273:107016 doi:10.1016/j.aquatox.2024.107016

Supplementary Files

This is a list of supplementary files associated with this preprint. Click to download.

- AoTKoornneefetalsupplementaldataNov2026FINAL.docx